RSC Advances

PAPER

View Article Online
View Journal | View Issue

Cite this: *RSC Adv.*, 2022, **12**, 32534

Co-encapsulation of paclitaxel and 5-fluorouracil in folic acid-modified, lipid-encapsulated hollow mesoporous silica nanoparticles for synergistic breast cancer treatment†

Huanli Yin, ‡[ab] Qi Yan, ‡[a] Yuan Liu,[a] Lan Yang,[a] Yang Liu,[a] Yujie Luo,[a] Tianyu Chen,[a] Ningxi Li[a] and Min Wu *[a]

Received 16th June 2022
Accepted 6th November 2022

DOI: 10.1039/d2ra03718a

rsc.li/rsc-advances

A dual-loaded multi-targeted drug delivery nanosystem was constructed to simultaneously load paclitaxel (PTX) and 5-fluorouracil (5-FU) for targeted delivery and sustained release at tumor sites. Hollow mesoporous silica nanoparticles (HMSNs) were prepared by the inverse microemulsion method, then modified with folic acid and pH- and temperature-responsive materials, co-loaded with PTX and 5-FU, and finally encapsulated into lipid membranes. The obtained nanosystem was selectively internalized by human breast cancer MCF-7 cells that overexpress folate receptors through an energy-dependent process, and it released both drugs *in vitro* in a simulated tumor microenvironment. Moreover, the inhibitory effect of the dual-loaded nanoparticles was significantly better than that of the free drugs, suggesting that the composite nanosystem has the potential to selectively target tumor sites and perform the synergistic effect of PTX and 5-FU, while reducing their toxic effects on normal tissues.

Introduction

Breast cancer is the malignant tumor with the highest incidence in women.[1] Current treatment strategies include surgical resection, radiation, and chemotherapy,[2] but their efficacy is low due to high drug resistance, toxicity, and hormonal interactions. Recent studies have shown that paclitaxel (PTX) and 5-fluorouracil (5-FU) can be synergistically used to treat breast and gastric cancer.[3–8] PTX is a hydrophobic drug commonly used for the treatment of breast, ovarian, and lung cancers.[9] However, its extremely poor water solubility requires the use of special solubilizers, such as Cremophor EL and absolute ethanol (1 : 1),[10] which lead to allergic reactions, significantly limiting the application of PTX in cancer treatment. 5-FU is a hydrophilic first-line chemotherapeutic widely used for the treatment of various malignancies. However, it must be administered repeatedly and intravenously due to poor oral bioavailability and short half-life, making it inconvenient and increasing the risk of toxic side effects.[11] Indeed, both PTX and 5-FU have low target specificity, so they can induce several adverse reactions, such as myelosuppression, allergies, and gastrointestinal complications.[12,13] In addition, they have different physicochemical properties and they require a fixed sequence of administration during combination therapy: PTX must be administered before long-term administration of 5-FU.[3,4,6,8] These two factors make their co-delivery and controlled release challenging in the clinic.

Hollow mesoporous silica nanoparticles (HMSNs) have a large surface area, high porosity, regular and ordered pore structure, uniform and adjustable pore size, as well as large pore volume and good biocompatibility, which endow them with the ability to carry and deliver drugs. The particle size of HMSNs is about 10–200 nm, which favors prolonged blood circulation *in vivo* and enhances passive targeting ability.[14] In addition, the HMSN surface consists of a large number of silyl hydroxyl groups, which enables their functionalization with tumor-specific biomolecules for active targeting and controlled drug release, such as folic acid (FA), monoclonal antibodies, glycoproteins, peptides, and nucleic acids.[15–17] Modification of HMSNs with groups that can participate in the enhanced permeability and retention (EPR) effect and react to the acidic pH (6–6.5) in the tumor tissue microenvironment can also favor the interactions between surface groups and drug molecules,[18] thereby improving their drug loading capacity and achieving sustained drug release.[19] However, further research is still needed to enhance the drug loading efficiency of such nanoparticles.[16,20]

[a]*School of Pharmacy, Chengdu Medical College, No. 783, Xindu Avenue, Xindu District, Chengdu, Sichuan Province, P. R. China. E-mail: wuminzhaofeng@126.com; Tel: +86-28-6230-8653*

[b]*Department of Pharmacy, West China Hospital, Sichuan University, Chengdu, Sichuan Province, P. R. China*

† Electronic supplementary information (ESI) available. See DOI: https://doi.org/10.1039/d2ra03718a

‡ Huanli Yin and Qi Yan share equal contribution.

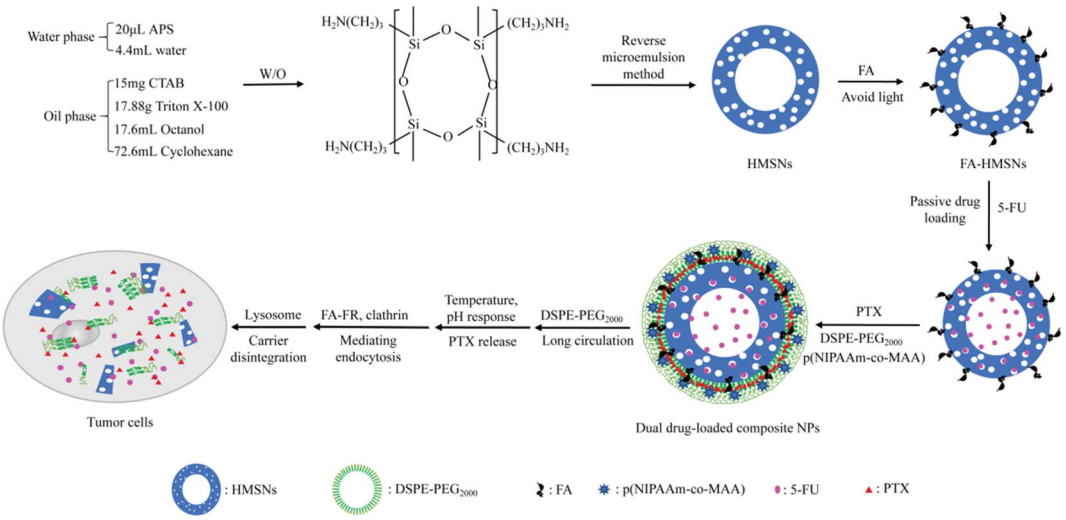

Scheme 1 Preparation of dual-modified hollow mesoporous silica nanoparticles (HMSNs) for the co-delivery of paclitaxel (PTX) and 5-fluorouracil (5-FU). APS, (3-aminopropyl)triethoxysilane; CTAB, cetyltrimethylammonium bromide; DSPE-PEG_{2000}, 1,2-distearoyl-*sn*-glycero-3-phosphatidyl ethanolamine-*N*-[methoxy(polyethylene glycol)$_{2000}$]; FA, folic acid; FR, folate receptor; p(NIPAAm-*co*-MAA), poly(*N*-isopropyl acrylamide-*co*-α-methacrylic acid).

To our knowledge, the co-loading of HMSNs with PTX and 5-FU has not yet been reported. In this study, we constructed a dual-loaded delivery system using PTX and 5-FU as model drugs for targeted synergistic breast cancer treatment (Scheme 1). HMSNs were synthesized using the inverse microemulsion method, then modified with FA to improve their internalization of breast cancer cells overexpressing folate receptors. After co-loading with 5-FU and PTX, the nanoparticle surface was modified with pH- and temperature-responsive materials for enhanced tumor targeted delivery and controlled drug release since tumor tissues have acidic microenvironment (pH 6–6.5) and higher temperature than normal tissues, then coated with a lipid membrane to improve permeability through biological membranes. The targeting specificity, cell selectivity and drug release properties of the FA-modified nanosystem were evaluated in human breast cancer MCF-7 cells overexpressing α-folate receptors, and evaluation in human hepatoma HepG2 cells underexpressing α-folate receptors was performed as a control.[21,22] The uptake mechanism and synergistic antitumor effect of the dual drug-loaded composite nanoparticles were also studied *in vitro*.

Experimental part

Materials

(3-Aminopropyl)triethoxysilane (APS), Triton X-100, tetraethyl orthosilicate (TEOS), (3-aminopropyl)trimethoxysilane, *N*-hydroxysuccinimide, *N*,*N*′-dicyclohexylcarbodiimide, triethylamine, 2,2′-azobisisobutyronitrile (AIBN), *N*-isopropylacrylamide (NIPAM), *n*-hexane, and 5-FU were purchased from Shanghai Aladdin Biochemical Polytron Technologies (Shanghai, China). Cetyltrimethylammonium bromide (CTAB), ammonium hydroxide solution, acetone, dimethyl sulfoxide (DMSO), α-methacrylic acid (MAA), chloroform, and ethanol were purchased from Chengdu Kelong Chemical Reagent Plant (Chengdu, China). FA and PTX were purchased from Wuhan Biocar Bio-Pharm Co., Ltd. (Wuhan, China). 1,2-Dipalmitoyl-*sn*-glycero-3-phosphocholine, 1,2-distearoyl-*sn*-glycero-3-phosphatidyl ethanolamine-*N*-[methoxy(polyethylene glycol)$_{2000}$] (DSPE-PEG_{2000}), cholesterol, and hydrogenated lecithin were purchased from Shanghai Yuanye Biotechnology Co., Ltd. (Shanghai, China). Fluorescein isothiocyanate (FITC) was obtained from BioFroxx (Einhausen, Germany) and the Cell Counting Kit-8 (CCK-8) from Dojindo China Co., Ltd. (Kumamoto, Japan). High-glucose Dulbecco's modified Eagle's medium (DMEM), RPMI1640 medium, and trypsin 0.25% (1×) were purchased from HyClone (Logan, CO, USA), phosphate-buffered saline (PBS) was from Wuhan Boster Biological Technology Co., Ltd. (Wuhan, China), and fetal bovine serum (FBS) was from Gibco (Uxbridge, UK). The Hoechst staining kit was purchased from the Beyotime Institute of Biotechnology (Jiangsu, China), and Annexin V-FITC/PI and cell cycle detection kits were purchased from Jiangsu KeyGEN BioTech Co., Ltd. (Jiangsu, China). All other reagents were of analytical grade and were used as obtained.

Human breast cancer cells (MCF-7) and human liver cancer cells (HepG2) were obtained from the Biomechanics and Nanomedicine Laboratory at the University of Electronic Science and Technology of China (Chengdu, China). Human breast cancer cells (MDA-MB-453, BT474) and human embryonic kidney cells (Hek-293t) were obtained from the State Key Laboratory of Biotherapy, Sichuan University (Chengdu, China). All cell lines were cultured in DMEM or RPMI1640 medium supplemented with 10% FBS and were incubated at 37 °C in a humidified atmosphere containing 5% CO_2.

Preparation of (5-FU+PTX)@FHPL

For the synthesis of 5-FU@FA-HMSNs@PTX@p(NIPAAm-*co*-MAA)@LB [(5-FU+PTX)@FHPL] nanoparticles, HMSNs were

first prepared by reverse microemulsion method following an existing protocol,[15,16] modified with FA, and loaded with 5-FU to obtain 5-FU@FA-HMSNs (ESI†). The optimum conditions for preparation of HMSNs and 5-FU@FA-HMSNs were studied (ESI†). The phospholipid film PTX@p(NIPAAm-*co*-MAA)@LB was also prepared using PTX, DSPE-PEG_{2000}, and the temperature- and pH-responsive copolymer p(NIPAAm-*co*-MAA), which was synthesized from NIPAM, MAA, and AIBN (ESI).[23] The NIPAM/MAA ratios were also investigated during the preparation of p(NIPAAm-*co*-MAA) (ESI). The doses of 5-FU and PTX were determined after evaluating their synergistic antitumor effect. Subsequently, 5-FU@FA-HMSNs (25 mg) were dissolved in 5 mL of deionized water and added to an eggplant-shaped flask covered with the PTX@p(NIPAAm-*co*-MAA)@LB film. After probe-sonication at 33 W (15 s on/off) for 20 min, the mixture was centrifuged at 14 942 g for 10 min and washed twice with deionized water. The resulting precipitate was dissolved in deionized water and dried *in vacuo* at 30 °C for 24 h to give (5-FU+PTX)@FHPL.

Similar processes were used to synthesize the following nanoparticles: FA-HMSNs@LB (FHL), FA-HMSNs@p(NIPAAm-*co*-MAA)@LB (FHPL), 5-FU@FA-HMSNs@PTX@LB [(5-FU+PTX)@FHL], 5-FU@HMSNs@PTX@p(NIPAAm-*co*-MAA)@LB [(5-FU+PTX)@HPL], 5-FU@FA-HMSNs@p(NIPAAm-*co*-MAA)@LB (5-FU@FHPL), FA-HMSNs@PTX@p(NIPAAm-*co*-MAA)@LB (PTX@FHPL), FITC@FA-HMSNs, and FITC@FA-HMSNs@p(NIPAAm-*co*-MAA)@LB (FITC@FHPL).

Nanoparticle characterization

The particle size distribution and zeta potential of the synthesized nanoparticles were determined by dynamic light scattering (DLS; Zetasizer Nano ZS 90, Malvern Instruments, Malvern, UK), and their morphology was observed by scanning electron microscopy (SEM; Sigma 300, Zeiss, Oberkochen, Germany) and transmission electron microscopy (TEM; JEM 2010, JEOL, Tokyo, Japan). The successful surface modification with FA was verified by Fourier-transform infrared spectroscopy (FTIR; Nicolet 380, Thermo Fisher Scientific, Waltham, MA, USA). N_2 adsorption/desorption isotherms were collected using a Micromeritics ASAP2020 sorptometer (Norcross, GA, USA) to determine the adsorption type and pore structure of HMSNs. FITC loading was assessed using a F-4500 fluorescence spectrophotometer (Hitachi, Tokyo, Japan), while thermogravimetric analysis of free drugs and nanoparticles was performed using a thermal gravimetric analyzer (TA Instruments, Milford, MA, USA). The lower critical solution temperature (LCST) of p(NIPAAm-*co*-MAA) was determined by differential scanning calorimetry (DSC200F3, Netzsch, Selb, Germany),[24,25] and the stability of the FHPL nanocarrier was examined in deionized water by determining the particle size.

In vitro drug release

Drug loading (DL) and encapsulation efficiency (EE) of 5-FU were determined using UV-visible spectrophotometry (Thermo Fisher Scientific, Madison, WI, USA) at 265 nm, while those of PTX were determined using high-performance liquid chromatography (Agilent Technologies, Santa Clara, CA, USA) at 227 nm using acetonitrile/water/methanol (36 : 41 : 23, v/v/v) as the mobile phase and C18 column as the stationary phase.

To determine the drug release profiles of (5-FU+PTX)@FHL and (5-FU+PTX)@FHPL *in vitro*, 100 mg of the nanoparticles was first dissolved in 20 mL of deionized water. Next, 1 mL of the resulting homogeneous suspension was placed into a pre-swelled dialysis bag with a molecular weight cutoff of 8000 Da. The dialysis bag was then immersed into 50 mL of phosphate-buffered solution containing 30% ethanol (pH 5.0, 6.8, 7.4) and placed in a constant temperature shaker. After shaking (100 rpm) at 37 °C or 41 °C, 5 mL aliquots were collected at 0.5, 1, 2, 6, 12, 18, 24, 36, and 48 h and replaced with the same volume of fresh buffer. Each experiment was performed in triplicate. DL and EE were calculated as follows:

$$\mathrm{EE}(\%) = \frac{\text{weight of drug in nanoparticles}}{\text{initial feeding amount of drug}} \times 100$$

$$\mathrm{DL}\ (\%) = \frac{\text{weight of drug in nanoparticles}}{\text{total weight of nanoparticles}} \times 100$$

Synergistic antitumor effect of free 5-FU and PTX

To study the ability of free PTX and 5-FU alone to inhibit the proliferation of breast and liver cancer cells, MCF-7 and HepG2 cells were seeded into 96-well plates (5×10^3 cells per well) and cultured overnight at 37 °C in RPMI1640 or DMEM, respectively, in an incubator containing 5% CO_2. Then the medium was discarded and 100 μL of fresh medium containing 5-FU or PTX (pre-dissolved in DMSO) at different concentrations was added. After incubation at 37 °C for 24 h, the medium was discarded, and cells were incubated with fresh medium and 10 μL of CCK-8 at 37 °C for 4 h. Optical density (OD) at 450 nm was measured using a microplate reader (VersaMax, Molecular Devices, San Jose, CA, USA), and cell viability was calculated using the formula:

$$\text{cell viability}(\%) = \frac{\text{OD of experimental group-OD of blank}}{\text{OD of control-OD of blank}} \times 100$$

Medium without drugs served as the control, while medium without drugs or cells served as the blank.

The synergistic inhibitory effect of 5-FU and PTX on MCF-7 cell proliferation at various concentrations was evaluated using the above method and the combination index (CI)-isobologram equation.[26] Dose-effect curves and CI values were calculated using CompuSyn©1.0 (ComboSyn, Paramus, NJ, USA).[27] The CI values were interpreted as follows: CI = 1, additive; CI < 1, synergistic; CI > 1, antagonistic.[26]

The same process was also used to determine the cytotoxicity of HMSNs, FA-HMSNs, and FHPL nanoparticles toward normal Hek-293t cells, HepG2 cells, and human breast cancer cells with different phenotypes (MCF-7, BT474, and MDA-MB-453). Double positive breast cancer MCF-7 cells express the

estrogen receptor (ER) and the progesterone receptor (PR) but not human epidermal growth factor receptor-2 (HER-2).[28] Double negative breast cancer MDA-MB-453 cells express HER-2 but not ER or PR.[29] Triple positive breast cancer BT474 cells express the ER, PR and HER-2.[28] The same procedure was also used to evaluate the inhibitory effect and tumor selectivity of (5-FU+PTX)@FHL, (5-FU+PTX)@HPL, and (5-FU+PTX)@FHPL against MCF-7 and HepG2 cells.

MCF-7 cell apoptosis

To examine the synergistic effect of the two drugs on cell apoptosis, 5-FU and PTX were dissolved in culture medium to prepare a series of solutions with various concentrations. MCF-7 cells were seeded into 12-well plates (2×10^5 cells per well) and incubated overnight at 37 °C. The medium was discarded, 1000 μL of the examined drug solution was added, and the plates were incubated for 24 h at 37 °C. The cells were then harvested with 500 μL of EDTA-free trypsin, resuspended in 500 μL of binding buffer, and stained with 5 μL of Annexin V-FITC and 5 μL of propidium iodide (PI) at room temperature for 15 min in the dark. Stained cells were detected by flow cytometry (NovoCyte 3130, ACEA Biosciences Inc, San Diego, CA, USA). Drug-free medium was used as the control. The same process was used to assess the effect of 5-FU@FHPL, PTX@FHPL, and (5-FU+PTX)@FHPL on the apoptosis of MCF-7 cells.

Nuclear morphology in MCF-7 cells

MCF-7 cells were seeded on coverslips in six-well plates (1×10^6 cells per well) and incubated overnight at 37 °C. The medium was discarded, 2000 μL of drug solution (prepared as described above) was added, and the plates were incubated for 24 h at 37 °C. Next, the solution was discarded and the isolated cells were washed twice with PBS and fixed with 500 μL of fixative solution for 15 min. The fixative solution was removed, the cells were washed twice with PBS and stained with 500 μL of Hoechst 33258 solution for 15 min. Finally, the staining solution was discarded, the cells were washed with PBS, and the coverslips with cells were placed onto glass slides containing 10 μL of anti-fluorescence quenching solution. Blue stained nuclei were observed with an inverted fluorescence microscope (IX71, Olympus Optical, Tokyo, Japan). The same process was used to investigate the effect of (5-FU+PTX)@FHPL on the morphology of MCF-7 cell nuclei.

Cell cycle arrest

0.5 μg mL^{-1} free 5-FU, 1 μg mL^{-1} free PTX, 2.5 μg mL^{-1} 5-FU@FHPL+2.5 μg mL^{-1} PTX@FHPL, and 5 μg mL^{-1} (5-FU+PTX)@FHPL were prepared using the culture medium. MCF-7 and HepG2 cells were seeded into six-well plates at a density of 1×10^7 cells per well and incubated overnight at 37 °C. Next, the medium was discarded, 2000 μL of the examined solution was added, and the plates were incubated for 24 h at 37 °C. The cells were then harvested with EDTA-free trypsin and resuspended in 300 μL of pre-chilled PBS. The resulting cell suspension was added dropwise to 700 μL of pre-chilled absolute ethanol, and the cells were fixed at 4 °C overnight. After centrifugation at 140 g for 3 min, the cells were washed twice with 1 mL of PBS and stained with 200 μL of PI/RNase A (9 : 1) at room temperature for 30–60 min in the dark. Stained cells were finally resuspended in PBS and detected by flow cytometry. Drug-free medium was used as the negative control.

Wound healing assay

Free 5-FU, free PTX, FHPL, and (5-FU+PTX)@FHPL were dissolved in culture medium (10 μg mL^{-1}). MCF-7 cells were seeded into six-well plates (5×10^4 cells per well) and incubated overnight at 37 °C. After the cells were completely attached and covered 90% of the well, the medium was discarded, and the cells were scratched with a pipette tip to create a wound about 1 mm wide.[30] Next, 1000 μL of the examined solution was added and the cells were incubated for 0, 6, 12, and 24 h, at which time they were photographed using an inverted fluorescence microscope. The relative wound area was calculated using Image-Pro Plus 6.0 software (Media Cybernetics, Santa Clara, CA, USA).[31] Drug-free medium was used as the negative control.

Cellular uptake

MCF-7 and HepG2 cells were seeded into six-well plates (1.6×10^5 cells per well) and incubated overnight at 37 °C. The medium was discarded and the cells were incubated at 37 °C for 30 min with 2000 μL of medium (negative control) or medium containing one of the following: 10 μg mL^{-1} chlorpromazine (CPZ), an inhibitor of clathrin-mediated endocytosis; 10 μg mL^{-1} filipin, an inhibitor of caveolae-mediated endocytosis; 5 μg mL^{-1} cytochalasin D, an inhibitor of actin-mediated endocytosis; or supersaturated FA. Other cultures were treated in the same ways but incubated at 4 °C for 30 min to serve as the low-temperature group. After incubation, drug solutions and medium were discarded, 1 mL of FITC@FHPL suspension (10 μg mL^{-1}) in fresh culture medium was added, and the plates were incubated at 37 °C or 4 °C for another 4 h. The medium was subsequently discarded, and the cells were washed twice with pre-cooled PBS and fixed with 500 μL of fixative solution for 15 min. The fixative solution was removed, and the cells were washed twice with PBS and observed using an inverted fluorescence microscope.

In some experiments, cells were washed twice with pre-cooled PBS, digested with 400 μL of 0.25% trypsin, washed again with pre-cooled PBS twice for 3 min each, then centrifuged at 700 g. The pelleted cells were resuspended in 0.5 mL of PBS and analyzed by flow cytometry.

Statistical analysis

Statistical analysis was performed using SPSS 13.0 (IBM, Chicago, IL, USA). All results were expressed as mean ± standard deviation (SD). Differences between two groups were evaluated for significance using two-way analysis of variance. Differences associated with $P < 0.05$ were considered statistically significant.

Results

Preparation and characterization of nanoparticles

The preparation of HMSNs was optimized using various reaction conditions and different doses of the core template APS

Table 1 Particle size distribution, polydispersity index, and zeta potential of various nanoparticles[a]

Nanoparticle	Size (nm)	Polydispersity index	Zeta potential (mV)
HMSNs	84.53 ± 1.58	0.16 ± 0.06	−22.23 ± 0.45
FA-HMSNs	103.73 ± 3.50	0.20 ± 0.15	−18.93 ± 0.75
FA-HMSNs@LB	145.23 ± 20.52	0.18 ± 0.09	−28.97 ± 0.49
FA-HMSNs@p(NIPAAm-*co*-MAA)@LB	205.33 ± 5.32	0.28 ± 0.16	−20.07 ± 1.53
5-FU@FA-HMSNs	105.50 ± 8.69	0.19 ± 0.03	−18.20 ± 0.50
5-FU@FA-HMSNs@PTX@p(NIPAAM-*co*-MAA)@LB	224.53 ± 6.18	0.19 ± 0.02	−16.50 ± 0.70
FITC@FA-HMSNs	134.14 ± 7.80	0.21 ± 0.02	−18.60 ± 1.25
FITC@FA-HMSNs@p(NIPAAM-*co*-MAA)@LB	215.26 ± 6.84	0.32 ± 0.14	−15.30 ± 1.28

[a] Data are shown as mean ± SD ($n = 3$). FA, folic acid; FITC, fluorescein isothiocyanate; 5-FU, 5-fluorouracil; HMSNs, hollow mesoporous silica nanoparticles; p(NIPAAm-*co*-MAA), poly(*N*-isopropyl acrylamide-*co*-α-methacrylic acid); PTX, paclitaxel.

and the pore-generating template CTAB (Table S1 and Fig. S1†). The preparation of 5-FU@FA-HMSNs was also optimized, and the highest DL and EE values were achieved when the FA-HMSNs/5-FU ratio was 1 : 2 and the reaction time was 24 h (Table S2†).

DLS measurements revealed that the average particle size of bare HMSNs increased after surface modification with FA (FA-HMSNs), after encapsulation into the lipid membrane (FA-HMSNs@LB), as well as after loading with FITC, 5-FU, and PTX. These results indicate that HMSNs can be effectively modified and loaded while maintaining their negative charge (Table 1). TEM and SEM also showed that drug-free HMSNs were regular hollow mesoporous spheres with a uniform size distribution and average sizes ranging between 59.76 ± 3.02 nm and 61.77 ± 5.20, good dispersibility, and no aggregation (Fig. 1A and C). A uniform lipid membrane around the nanoparticles was observed after drug loading (Fig. 1B). The particle size of 5-FU@FA-HMSNs, FITC@FA-HMSNs, FITC@FHPL, and (5-FU+PTX)@FHPL was within the range of the EPR effect (Table 1), suggesting that they could be used for passive targeting.

The successful synthesis of HMSNs was verified based on the characteristic FTIR absorption peaks of SiO_2 at 459, 801, and 1050 cm^{-1}. FA modification was also confirmed based on the characteristic FTIR absorption peaks of the amide bond at

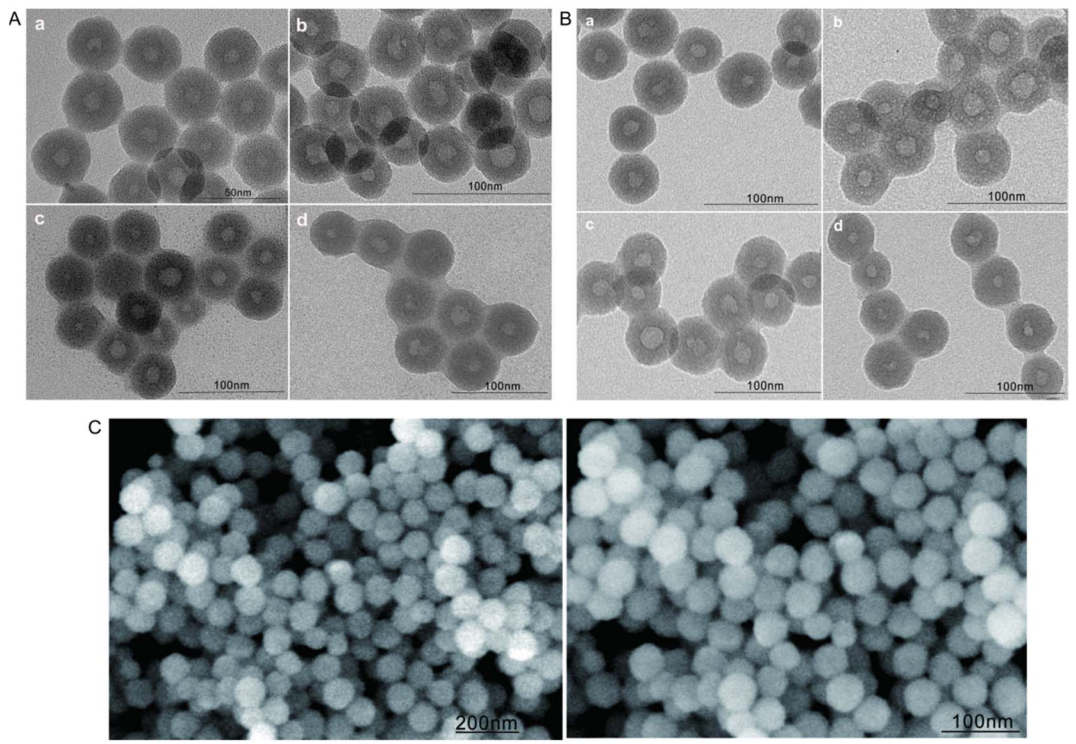

Fig. 1 Transmission electron micrographs of (A) drug-free nanoparticles [(a) HMSNs, (b) FA-HMSNs, (c) FA-HMSNs@LB, (d) FA-HMSNs@p(NIPAAm-*co*-MAA)@LB] and (B) drug-loaded nanoparticles [(a) 5-FU@FA-HMSNs, (b) 5-FU@FA-HMSNs@p(NIPAAm-*co*-MAA)@LB, (c) FITC@FA-HMSNs@p(NIPAAm-*co*-MAA)@LB, (d) 5-FU@FA-HMSNs@PTX@p(NIPAAm-*co*-MAA)@LB]. (C) Scanning electron micrographs of HMSNs. FA, folic acid; FITC, fluorescein isothiocyanate; 5-FU, 5-fluorouracil; HMSNs, hollow mesoporous silica nanoparticles; p(NIPAAm-*co*-MAA), poly(*N*-isopropyl acrylamide-*co*-α-methacrylic acid); PTX, paclitaxel.

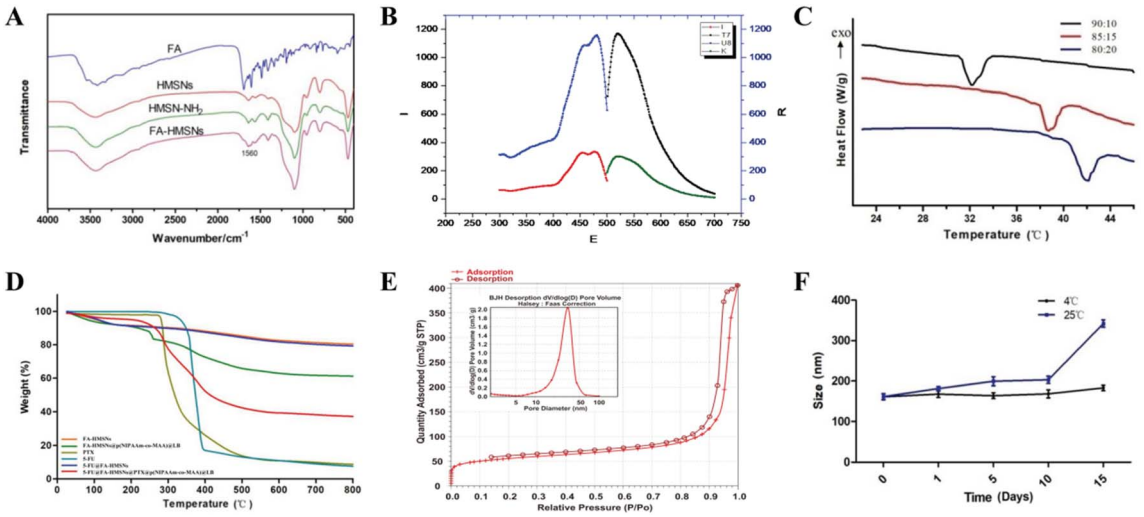

Fig. 2 (A) Fourier-transform infrared spectra of FA, HMSNs, HMSN-NH_2, and FA-HMSNs. (B) Fluorescence spectra of free FITC (blue curve) and FITC@FA-HMSNs (red curve). (C) Differential scanning calorimetry curves of poly(*N*-isopropyl acrylamide-*co*-α-methacrylic acid) [p(NIPAAm-*co*-MAA)]. (D) Thermogravimetric analysis of free drugs and various nanoparticles. (E) N_2 adsorption/desorption isotherms and pore size distribution of HMSNs. (F) Changes in the particle size of FA-HMSNs@p(NIPAAm-*co*-MAA)@LB (FHPL) over time at different temperatures. Data are shown as mean ± SD (n = 3). FA, folic acid; FITC, fluorescein isothiocyanate; 5-FU, 5-fluorouracil; HMSNs, hollow mesoporous silica nanoparticles; PTX, paclitaxel.

1560 cm^{-1} (Fig. 2A), indicating that FA conjugated to HMSNs *via* an amide bond. Free FITC and FITC@FA-HMSNs showed the same characteristic fluorescence peaks (Fig. 2B), indicating that FITC was successfully loaded on FA-HMSNs.

Differential scanning calorimetry showed that the LCST of p(NIPAAm-*co*-MAA) varied significantly depending on the NIPAM/MAA ratio. Interestingly, when the ratio was 85 : 15, the LCST of the polymer (38.95 °C) was close to the temperature of tumor tissues, thus was chosen as the optimum ratio for preparation of p(NIPAAm-*co*-MAA) (Fig. 2C). The polymer also formed a clear and transparent solution in deionized water at room temperature, but a white precipitate was observed when the temperature was above the LCST (Fig. S2†); the polymer gradually redissolved when the temperature dropped to room temperature. In addition, thermogravimetric analysis showed that the weight of FA-HMSNs, 5-FU@FA-HMSNs, and (5-FU+PTX)@FHPL decreased with increasing temperature by about 20%, 25%, and 62%, respectively (Fig. 2D), indicating the successful modification of FA-HMSNs with p(NIPAAm-*co*-MAA).

According to the IUPAC classification, the N_2 adsorption/desorption isotherms of HMSNs were typical type IV isotherms with an obvious H1 hysteresis loop at P/P_o = 0.8–1.0 (Fig. 2E), confirming that HMSNs had a hollow, mesoporous structure. Using the Barret–Joyner–Halenda method, we determined the average pore diameter of HMSNs to be 21.85 ± 1.21 nm, the Brunauer–Emmett–Teller surface area to be 188.39 ± 2.35 m^2 g^{-1}, and the average pore volume to be 2.55 ± 0.46 cm^3 g^{-1}. These results indicate that HMSNs contained a large hollow volume, a large mesopore volume and a large specific surface area; these characteristics are highly desirable for drug loading.

The FHPL nanoparticles were also dissolved in deionized water, and changes in their particle size were monitored for 15 days at room temperature and 4 °C. Although significant aggregation was observed at 25 °C over time, the particle size remained almost unchanged at 4 °C (Fig. 2F), suggesting that the nanocarriers should be stored at low temperature. We also found that the FHPL nanoparticles remained stable for 24 h at room temperature in PBS, saline, RPMI1640 medium, and DMEM (Fig. S3†).

In vitro drug release

The DL and EE values of 5-FU in FA-HMSNs were calculated at 28.49 ± 3.25% and 20.52 ± 3.31%, respectively (Table S2†), while the DL of PTX in (5-FU+PTX)@FHPL was 14.29 ± 2.11%, and the EE of PTX was close to 100% since it was completely loaded in the lipid membrane. In addition, the maximum release rate of 5-FU from (5-FU+PTX)@FHL and (5-FU+PTX)@FHPL at 37 °C and pH 5.0 was 11.34 ± 5.21%, while that of PTX was 15.15 ± 4.47%. Lower rates were observed at the same temperature but higher pH of 6.8 or 7.4 (Fig. 3A–D), indicating that both nanocarriers were stable under physiological conditions and might have fewer toxic effects on normal tissues and organs. In contrast, the release rate of PTX from (5-FU+PTX)@FHPL at pH 5.0 and 41 °C reached about 50% within 6 h and 85.68 ± 5.52% within 48 h (Fig. 3H). Similarly, the release rate of 5-FU under the same conditions reached ~40% within 12 h and 82.45 ± 4.31% within 48 h (Fig. 3F). However, when the pH increased to 6.8 or 7.4, (5-FU+PTX)@FHPL showed weaker drug release properties than at pH 5.0, indicating that the (5-FU+PTX)@FHPL nanoplatform has good pH- and temperature-responsive properties and has the potential to release both drugs in the tumor microenvironment in a targeted, sustained manner.

The drug release curves of (5-FU+PTX)@FHPL at 41 °C and pH 5.0 were also fitted to six commonly used *in vitro* models of

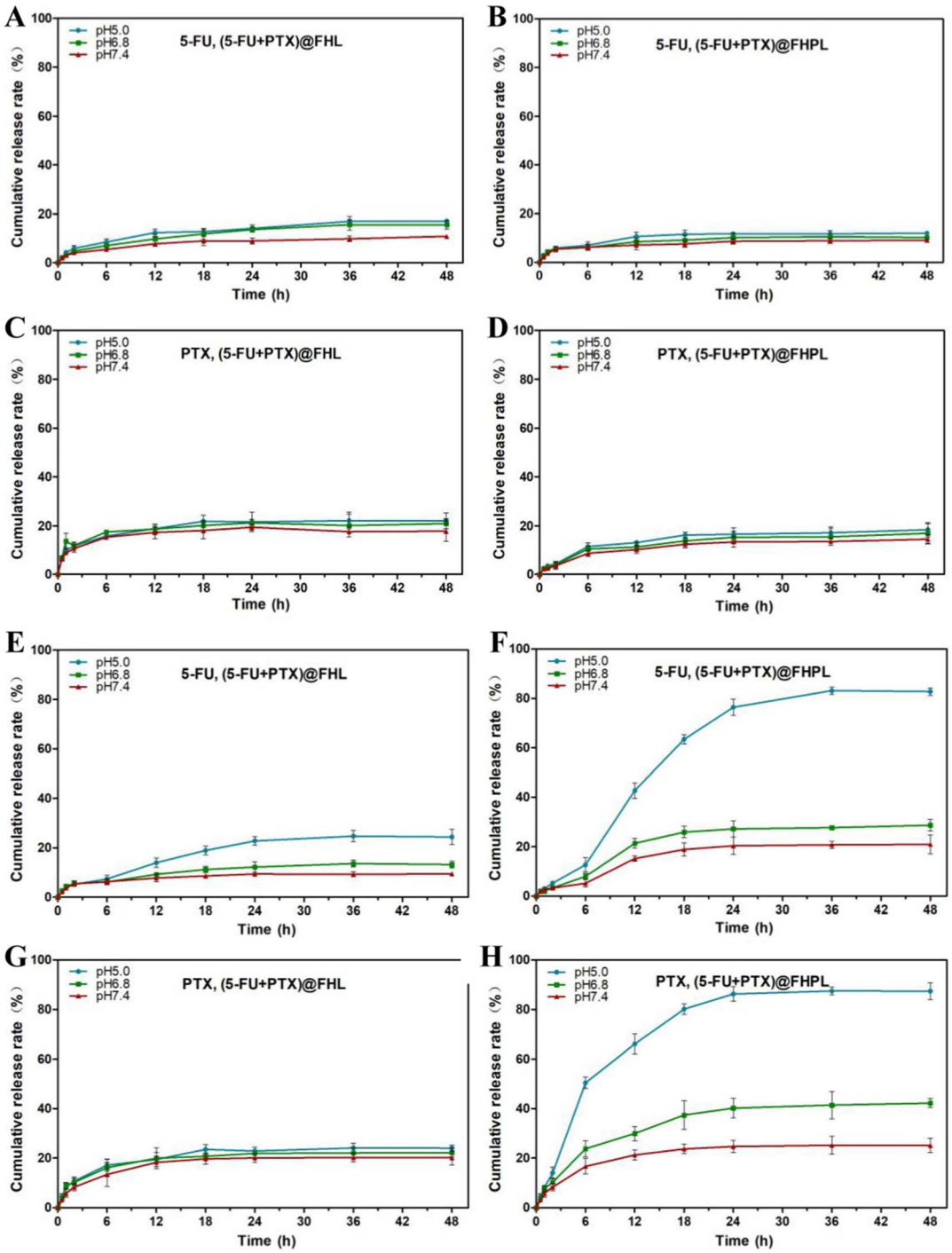

Fig. 3 *In vitro* release profiles of 5-fluorouracil (5-FU) and paclitaxel (PTX) from 5-FU@FA-HMSNs@PTX@LB [(5-FU+PTX)@FHL] and 5-FU@FA-HMSNs@PTX@p(NIPAAm-*co*-MAA)@LB [(5-FU+PTX)@FHPL] at (A–D) 37 °C and (E–H) 41 °C. Data are shown as mean ± SD ($n = 3$). HMSNs, hollow mesoporous silica nanoparticles; p(NIPAAm-*co*-MAA), poly(*N*-isopropyl acrylamide-*co*-α-methacrylic acid).

sustained drug release preparations using Origin Plus 2016 software (Table S3 and Fig. S5†).[32–36] Goodness of fit (R^2) indicated that the *in vitro* release of 5-FU and PTX fitted well into all models except the zero-order dynamics model, suggesting that (5-FU+PTX)@FHPL can release both drugs in a sustained manner through diffusion and erosion processes.

Inhibitory effect of free 5-FU and PTX on cell proliferation

The effects of free 5-FU and PTX, alone or in combination, on tumor cell proliferation were assessed using the CCK-8 assay. Both free drugs inhibited the proliferation of MCF-7 and HepG2 cells in a concentration- and time-dependent manner, while the optimum activity was observed after treatment for

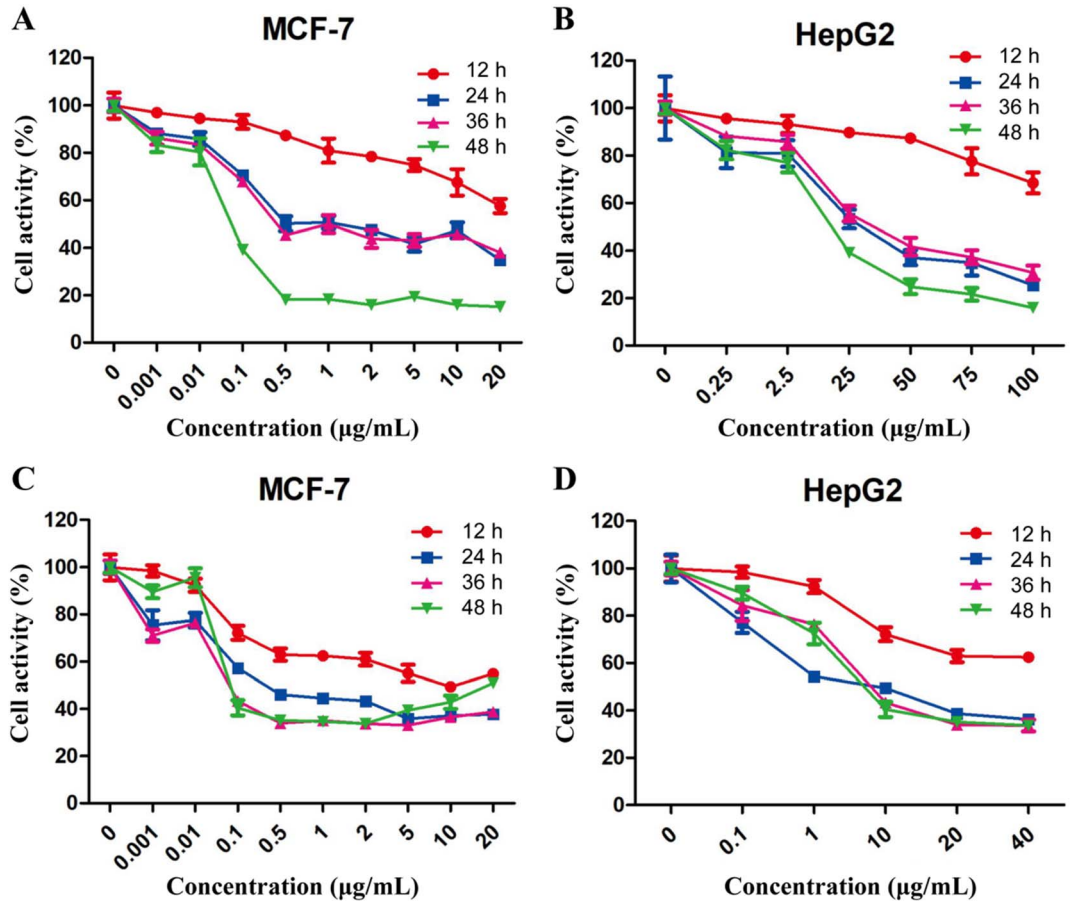

Fig. 4 Viability of MCF-7 and HepG2 cells after treatment with (A and B) free 5-fluorouracil or (C and D) free paclitaxel, as determined using the Cell Counting Kit-8 assay. Data are shown as mean ± SD ($n = 3$).

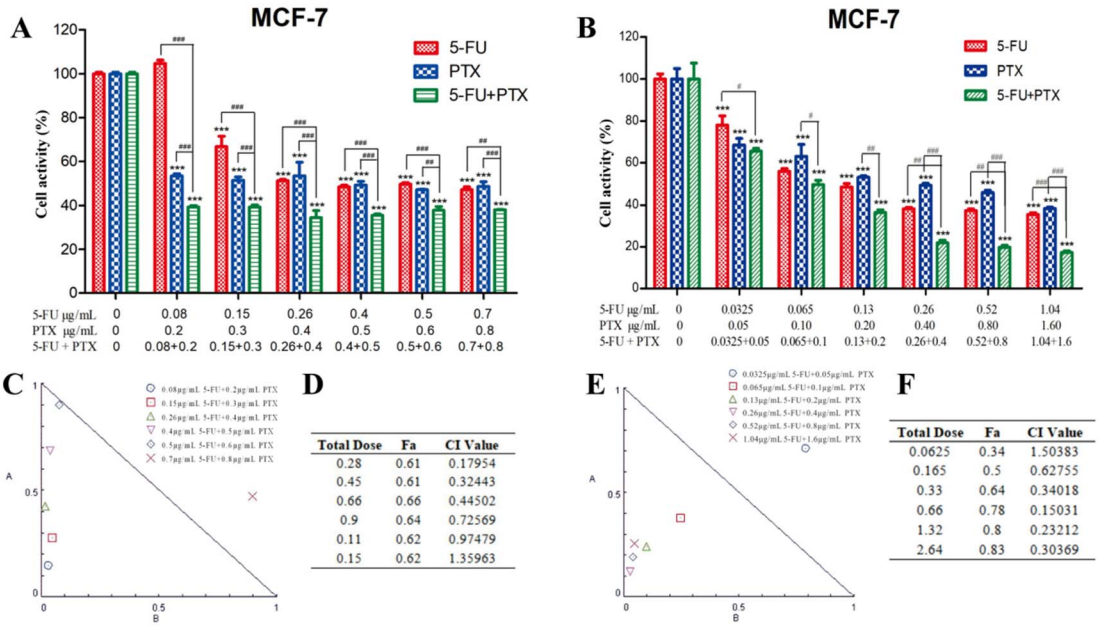

Fig. 5 (A and B) Synergistic inhibitory effect of 5-fluorouracil (5-FU) and paclitaxel (PTX) on the viability of MCF-7 cells after 24 h treatment, when the drugs were mixed at (*A*) different ratios or (B) a fixed ratio of 13 : 20. $^{*}P < 0.05$, $^{**}P < 0.01$, $^{***}P < 0.001$ *vs.* control. $^{\#}P < 0.05$, $^{\#\#}P < 0.01$, $^{\#\#\#}P < 0.001$ (two-way analysis of variance). (C and E) Isobologram of cell viability after treatment with both drugs (C) at different ratios or (E) at a constant ratio of 5-FU/PTX = 13 : 20. (D and F) Combination index (CI) values calculated after treatment with both drugs (D) at different ratios or (F) at a constant ratio of 5-FU/PTX = 13 : 20. Data are shown as mean ± SD ($n = 3$). Fa, fraction affected; 5-FU, 5-fluorouracil; PTX, paclitaxel.

24 h (Fig. 4). The IC_{50} values for 5-FU were 0.26 μg mL^{-1} against MCF-7 cells and 5.0 μg mL^{-1} against HepG2 cells, while the corresponding values for PTX were 0.4 μg mL^{-1} and 1.2 μg mL^{-1}. These results indicate that free 5-FU and PTX have a better inhibitory effect on MCF-7 cells than on HepG2 cells.

Compared to each drug on its own, the combination of 5-FU and PTX at different ratios had a better inhibitory effect on MCF-7 cell proliferation at 24 h, but no significant increase was observed with increasing drug dosage (Fig. 5A). Five points corresponding to 5-FU/PTX ratios of 1 : 2, 2 : 5, 4 : 5, 5 : 6, and 13 : 20 were below the line of 1 in the respective isobologram (Fig. 5C and D), suggesting that the two drugs synergistically inhibited the proliferation of MCF-7 cells. When the 5-FU/PTX ratio was set at 13 : 20, the inhibitory effect of the 5-FU+PTX group was significantly better than that of the individual drugs at all concentrations examined (Fig. 5B). The isobologram demonstrated a synergistic effect at all concentrations except 0.0625 μg mL^{-1} (Fig. 5E and F).

The synergistic effect of 5-FU and PTX on MCF-7 cell apoptosis was further assessed using PI/Annexin V-FITC double staining and flow cytometry. The combined application of 5-FU and PTX at two different concentrations led to an apoptosis rate of around 27%, which was considerably higher than that of either drug on its own (5-FU: 10.4% and 12.5%; PTX: 15.8% and 19.1%) (Fig. 6A), confirming their synergistic inhibitory activity.

The nuclei of MCF-7 cells treated with both drugs were also stained with Hoechst 33258 and observed by fluorescence microscopy (Fig. 6B). The nuclei in the control group had

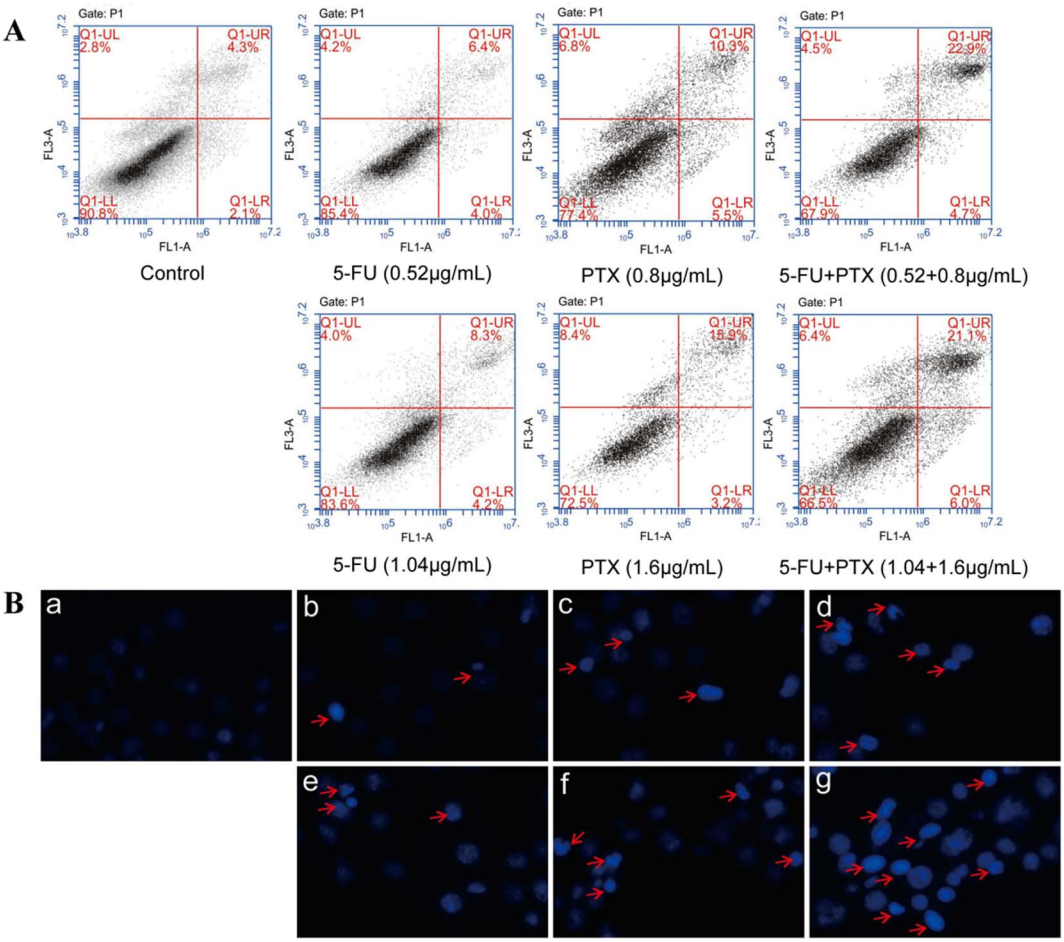

Fig. 6 (A) Apoptosis of MCF-7 cells after treatment with different concentrations of 5-fluorouracil (5-FU) and paclitaxel (PTX), alone or in combination, as determined by PI/Annexin V-FITC staining and flow cytometry. Q1-upper left, PI^+ (cells undergoing necrosis); Q1-upper right, Annexin V-FITC + PI^+ (cells in late apoptosis and secondary necrosis); Q1-lower right, Annexin V-FITC + PI^- (cells in early apoptosis); Q1-lower left, Annexin V-FITC − PI^- (living cells). The total apoptotic rate was calculated as the sum of the proportions in the Q1-upper right and Q1-lower right areas. (B) MCF-7 cell nuclei stained with Hoechst 33258 (magnification, 20×) after treatment for 24 h with (a) control (0 μg mL^{-1}), (b) 5-FU (0.52 μg mL^{-1}), (c) PTX (0.8 μg mL^{-1}), (d) 5-FU (0.52 μg mL^{-1}) + PTX (0.8 μg mL^{-1}), (e) 5-FU (1.04 μg mL^{-1}), (f) PTX (1.6 μg mL^{-1}), or (g) 5-FU (1.04 μg mL^{-1}) + PTX (1.6 μg L^{-1}). Red arrows indicate chromatin condensation, nuclear fragmentation, and apoptotic bodies. All conditions were analyzed in triplicate in at least three independent experiments. FITC, fluorescein isothiocyanate; PI, propidium iodide.

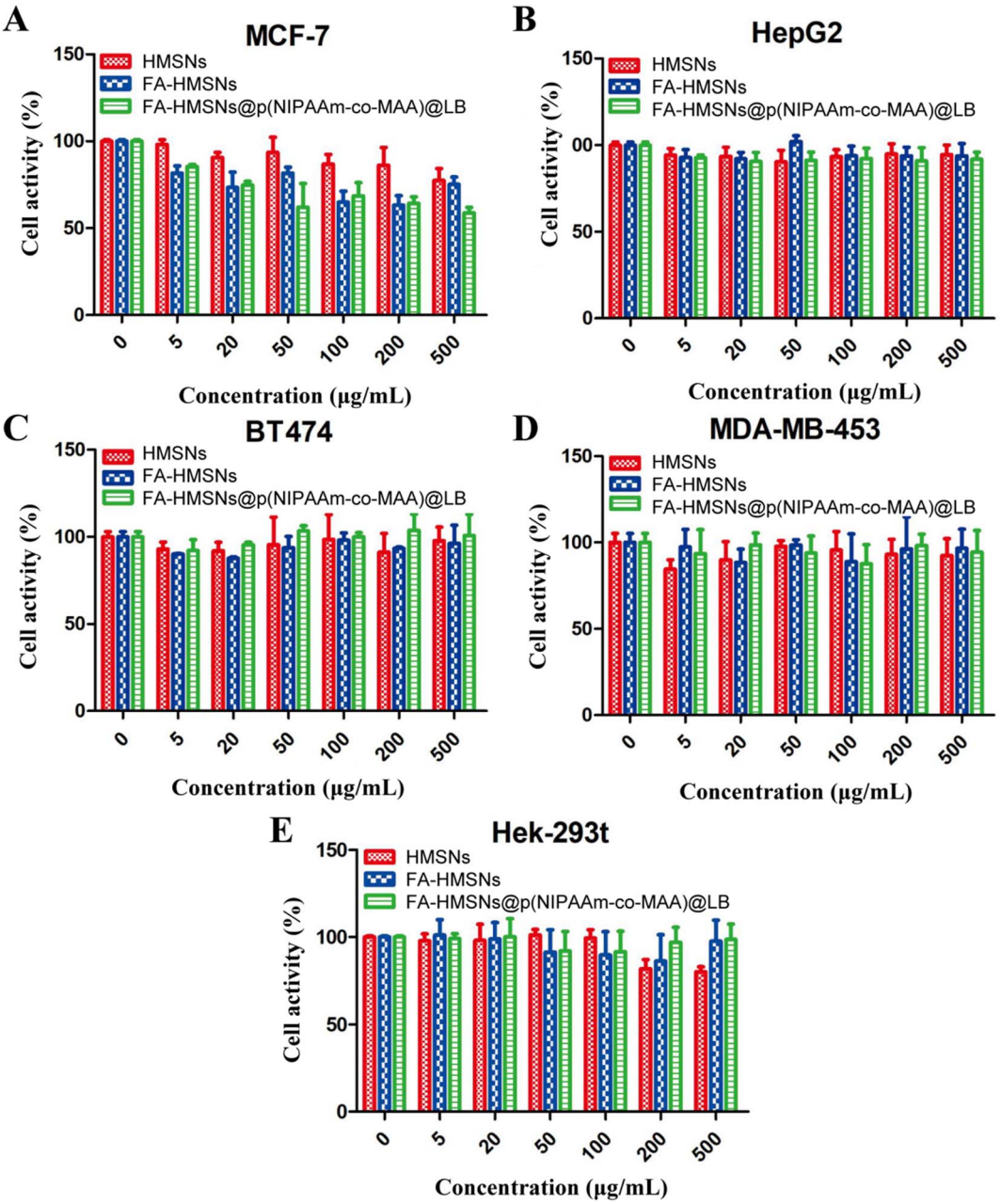

Fig. 7 Cytotoxicity of hollow mesoporous silica nanoparticles (HMSNs), FA-HMSNs, and FA-HMSNs@p(NIPAAm-*co*-MAA)@LB nanoparticles against (A) MCF-7 cells, (B) HepG2 cells, (C) BT474 cells, (D) MDA-MB-453 cells and (E) normal Hek-293t cells. Data are shown as mean ± SD (n = 3). FA, folic acid; p(NIPAAm-*co*-MAA), poly(*N*-isopropyl acrylamide-*co*-α-methacrylic acid).

a regular or nearly round shape and uniform size, and the blue color was evenly distributed. In contrast, cell nuclei in the drug-treated groups were densely stained, while some nuclei appeared to shrink and divide, indicating that 5-FU and PTX can effectively induce cancer cell apoptosis.

Cytotoxicity of drug-free nanoparticles

Drug-free nanoparticles showed no significant cytotoxicity against normal or tumor cells, suggesting the safety of HMSNs (Fig. 7). FHPL nanoparticles were more cytotoxic to MCF-7 cells than HMSNs and FA-HMSNs (Fig. 7A) but less cytotoxic to normal Hek-293t cells (Fig. 7E), suggesting that they can be used to selectively target MCF-7 cells.

Inhibitory effect of (5-FU+PTX)@FHPL on tumor cell proliferation

The proliferation of MCF-7 and HepG2 cells was significantly reduced after treatment with six different formulations. In particular, MCF-7 cells treated with (5-FU+PTX)@FHPL for 24 and 48 h showed significantly lower proliferation than cells

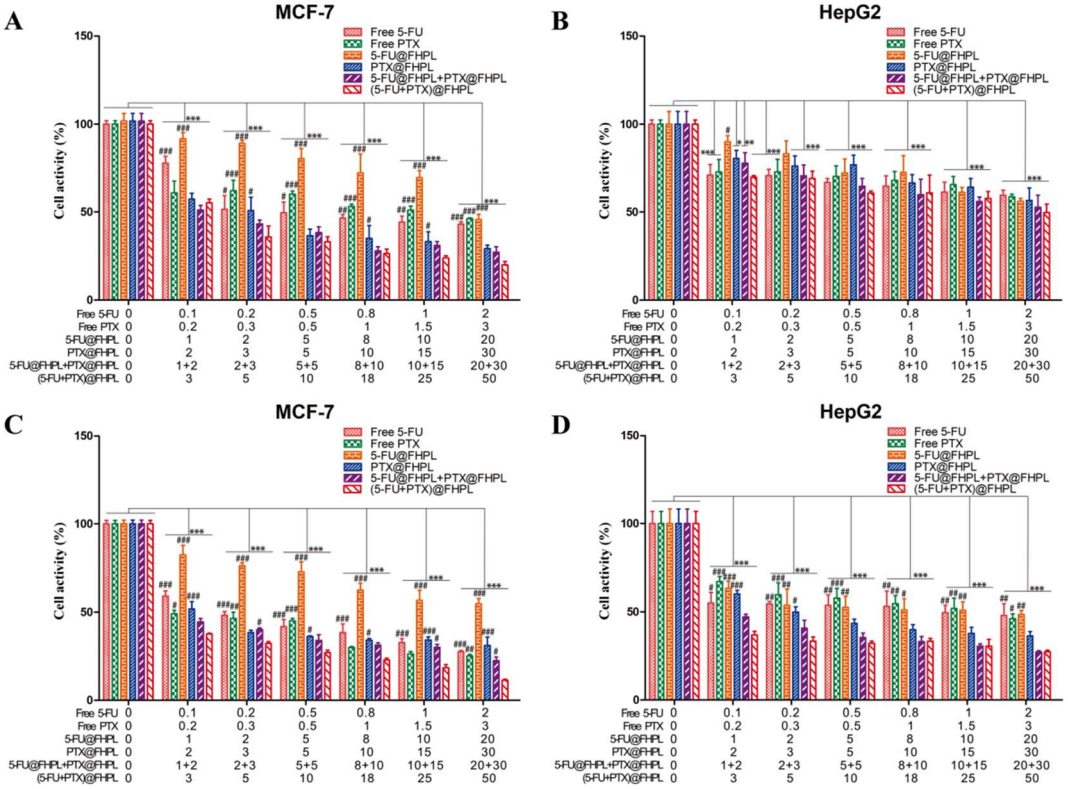

Fig. 8 Proliferation of MCF-7 and HepG2 cells after treatment with various doses of free drugs and drug-loaded nanoparticles for (A-B) 24 h and (C-D) 48 h. $^{*}P < 0.05$, $^{**}P < 0.01$, $^{***}P < 0.001$ *vs.* control. $^{\#}P < 0.05$, $^{\#\#}P < 0.01$, $^{\#\#\#}P < 0.001$ (difference between free 5-FU, free PTX, 5-FU@FHPL, PTX@FHPL, 5-FU@FHPL+PTX@FHPL and (5-FU+PTX)@FHPL nanoparticles; two-way analysis of variance). Data are shown as mean ± SD ($n = 3$). 5-FU, 5-fluorouracil; PTX, paclitaxel.

treated with free 5-FU, free PTX, 5-FU@FHPL, or PTX@FHPL at most concentrations, and significant difference was observed between the (5-FU+PTX)@FHPL and 5-FU@FHPL+PTX@FHPL groups at three concentrations after treatment for 48 h (Fig. 8A and C). Similar results were obtained for HepG2 cells treated with (5-FU+PTX)@FHPL for 48 h, however, no significant difference was observed between HepG2 cells treated with (5-FU+PTX)@FHPL and 5-FU@FHPL+PTX@FHPL (Fig. 8D). Besides, almost no significant difference was observed between the (5-FU+PTX)@FHPL group and the other five groups after treatment for 24 h (Fig. 8B), suggesting that the dual-loaded nanoparticles exert stronger effects against MCF-7 cells than against HepG2 cells.

Tumor cell selectivity

(5-FU+PTX)@FHL, (5-FU+PTX)@HPL, and (5-FU+PTX)@FHPL at concentrations of 0–50 μg mL^{-1} had insignificantly different inhibitory effects on MCF-7 cell proliferation after 24 h of treatment (Fig. 9A), as well as on HepG2 cell proliferation after 24 and 48 h (Fig. 9B and D). (5-FU+PTX)@FHPL at concentrations of 10, 20, 30, or 50 μg mL^{-1} had a significantly stronger inhibitory effect against MCF-7 cells compared to the other two groups after 48 h of treatment (Fig. 9C), indicating that the dual-modified nanoparticles can selectively inhibit the proliferation of MCF-7 cells.

Effect of drug-loaded FHPL nanoparticles on tumor cell apoptosis

To examine the effect of the developed formulations on cell apoptosis, MCF-7 cells treated with drug-loaded nanoparticles were stained with PI/Annexin V-FITC and analyzed by flow cytometry. Treatment of MCF-7 cells with 5 or 10 μg mL^{-1} (5-FU+PTX)@FHPL for 24 h resulted in respective apoptosis rates of 26.15% and 35.85%, which were considerably higher than those achieved with 5-FU@FHPL (8.27% and 23.48%) and PTX@FHPL (17.09% and 26.96%), suggesting that 5-FU and PTX act synergistically to induce apoptosis in cancer cells (Fig. 10A).

The nuclei of MCF-7 cells treated with (5-FU+PTX)@FHPL were also stained with Hoechst 33258 and observed by fluorescence microscopy. Cell nuclei in the control group had uniform size and regular or nearly round shape, and the blue color was evenly distributed. In contrast, the nuclei in the drug-treated groups were densely stained, while some of them appeared to shrink or divide, confirming that (5-FU+PTX)@FHPL can effectively induce apoptosis in MCF-7 cells (Fig. 10B).

Cell cycle arrest

Free drugs and drug-loaded nanoparticles effectively blocked the cell cycle at the S phase in MCF-7 cells, with (5-FU+PTX)@FHPL showing a more significant effect (Fig. 11A and B). Some cells were also detected in the sub-G1 phase, probably due to cell

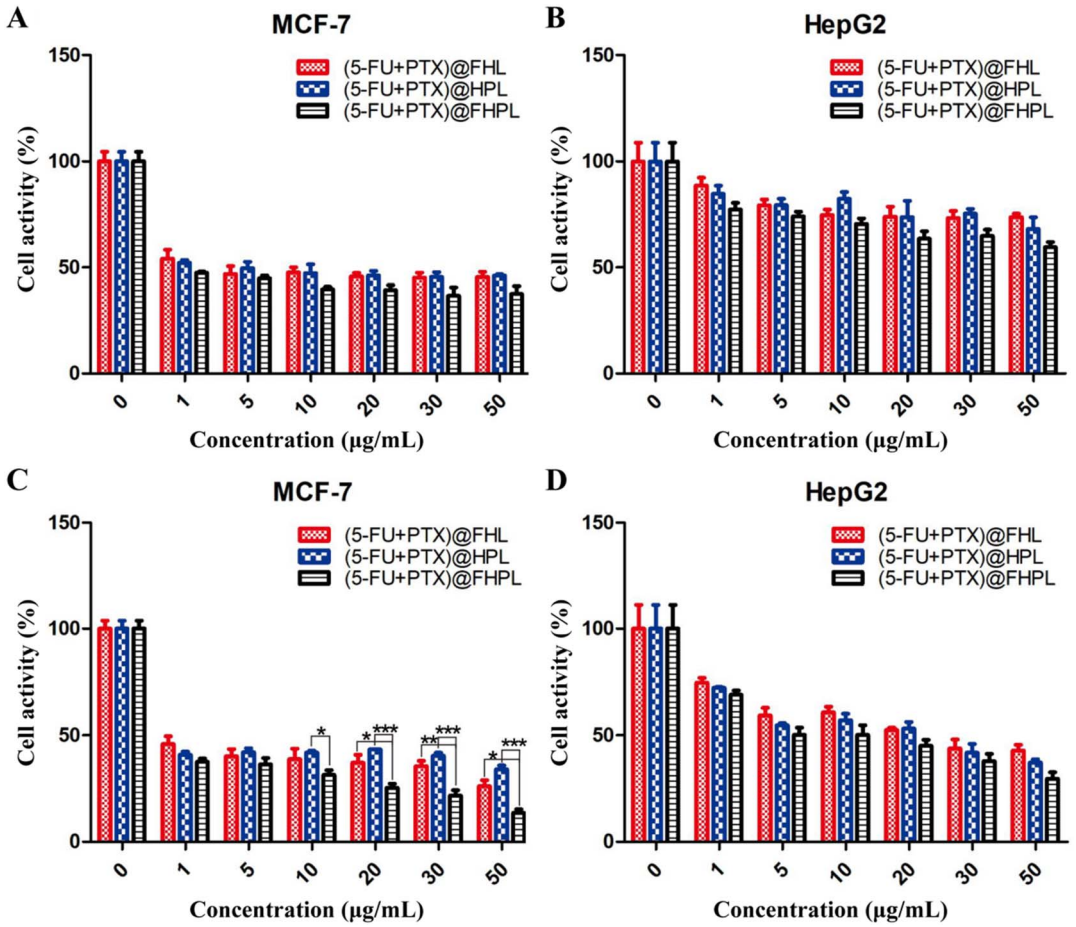

Fig. 9 Effect of single- and dual-modified nanoparticles on the proliferation of MCF-7 and HepG2 cells after treatment for (A and B) 24 h and (C and D) 48 h. *P < 0.05, **P < 0.01, ***P < 0.001 (two-way analysis of variance). Data are shown as mean ± SD (n = 3). 5-FU, 5-fluorouracil; PTX, paclitaxel.

apoptosis induced by (5-FU+PTX)@FHPL. In contrast, none of the examined formulations induced cell cycle arrest in HepG2 cells (Fig. 11C and D), suggesting that (5-FU+PTX)@FHPL nanoparticles can selectively induce cell cycle arrest in MCF-7 cells.

Wound healing

Wounds in the control and FHPL-treated groups were completely healed after 24 h treatment (Fig. 12). In contrast, only 20% of wound healing was achieved in the free drug-treated groups, suggesting that 5-FU and PTX can partially inhibit the migration of MCF-7 cells. Interestingly, (5-FU+PTX)@FHPL further hindered the wound healing process after 24 h treatment, indicating that the two drugs act synergistically to inhibit cell migration.

Cellular uptake

In order to investigate the cellular uptake of the prepared nanoparticles, MCF-7 and HepG2 cells were treated with FITC@FHPL, and the green fluorescence of FITC was observed by fluorescence microscopy. The uptake of FITC@FHPL was significantly inhibited in the low-temperature group (Fig. 13A and C), suggesting that the nanoparticle endocytosis is an active, energy-dependent process. In addition, CPZ, filipin, and cytochalasin D significantly reduced the uptake of nanoparticles by HepG2 cells compared to control, indicating that the nanoparticles enter HepG2 cells through clathrin-, caveolae- and actin-mediated endocytosis. In contrast, CPZ, but not filipin or cytochalasin D, significantly reduced the uptake of FITC@FHPL by MCF-7 cells, suggesting that the developed nanoparticles enter MCF-7 cells through a clathrin-mediated process. Furthermore, we found that supersaturated FA significantly inhibited the uptake of FITC@FHPL by MCF-7 cells but not by HepG2 cells, indicating that the nanoparticles were internalized by MCF-7 cells through folate receptor-mediated endocytosis. These results were confirmed by flow cytometry (Fig. 13B and D) and semi-quantification of flow cytometry results (Fig. 13E).

Discussion

In this study, we constructed a composite nanoplatform with large hollow and mesopore volume and high specific surface

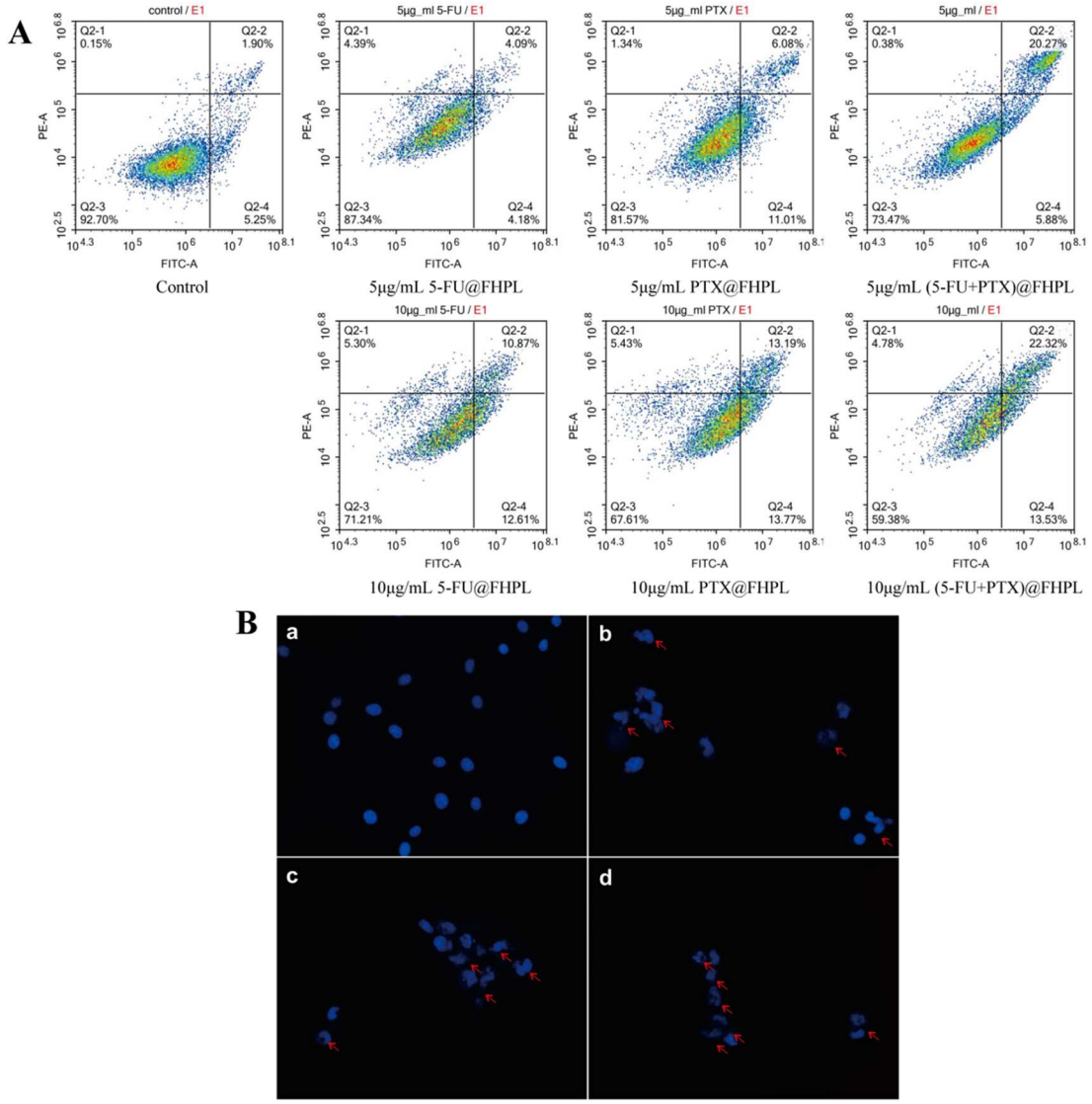

Fig. 10 (A) Apoptosis of MCF-7 cells after treatment with single- or dual-loaded nanoparticles, as determined by PI/Annexin V-FITC staining and flow cytometry. Q1-upper left, PI^+ (cells undergoing necrosis); Q1-upper right, Annexin V-FITC + PI^+ (cells in late apoptosis and secondary necrosis); Q1-lower right, Annexin V-FITC + PI^- (cells in early apoptosis); Q1-lower left, Annexin V-FITC − PI^- (living cells). The total apoptotic rate was calculated as the sum of the proportions in the Q1-upper right and Q1-lower right areas. (B) MCF-7 cell nuclei stained with Hoechst 33258 (magnification, 20×) after treatment with (5-FU+PTX)@FHPL [(a) 0 μg mL^{-1} (control), (b) 5 μg mL^{-1}, (c) 10 μg mL^{-1}, (d) 20 μg mL^{-1}]. Red arrows indicate chromatin condensation, nuclear fragmentation, and apoptotic bodies. All conditions were analyzed in triplicate in at least three independent experiments. FITC, fluorescein isothiocyanate; 5-FU, 5-fluorouracil; PI, propidium iodide; PTX, paclitaxel.

area for the targeted co-delivery of chemotherapeutic drugs with different physicochemical properties.

At first, HMSNs were modified with FA to reduce their internalization by normal cells and enhance their targeting ability to tumor cells, such as MCF-7, which are known to overexpress α-folate receptors. Our results revealed that (5-FU+PTX)@FHPL nanoparticles can specifically target MCF-7 cells over HepG2 cells and induce cell apoptosis and cell cycle arrest. Similarly, another group has developed shape-controlled HMSNs modified with polyethylene glycol and FA, which selectively targeted human cervical cancer HeLa cells over-expressing α-folate receptors.[37] According to this, our FHPL nanoparticles may have application prospects in the synergistic treatment of cervical cancer and other tumors which over-express α-folate receptors.

In order to achieve controlled drug release in the tumor microenvironment and reduce toxic side effects on normal tissues, the HMSNs were also modified with the pH- and temperature-responsive polymer p(NIPAAm-*co*-MAA).[38] Furthermore, the nanoparticles were encapsulated into lipid membranes to improve the poor solubility of PTX and enhance biocompatibility.[38–40] Another group constructed a carrier consisting of lipid-coated hollow mesoporous silica nanospheres (L-HMSNs) for co-delivery of doxorubicin (DOX) and PTX to

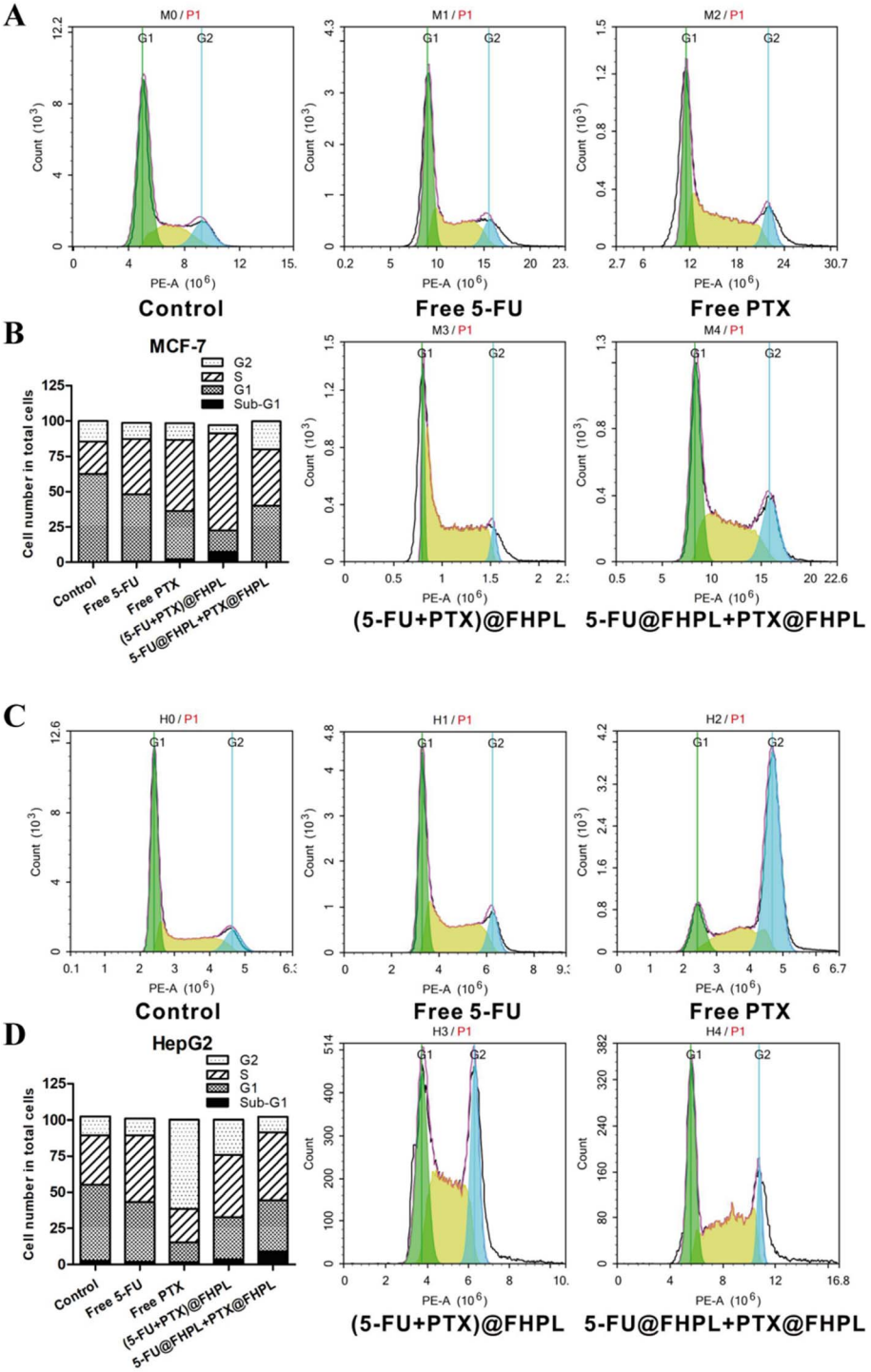

Fig. 11 Effect of free 5-fluorouracil (5-FU), free paclitaxel (PTX), (5-FU@FHPL+PTX@FHPL), and (5-FU+PTX)@FHPL on cell cycle arrest in (A and B) MCF-7 and (C and D) HepG2 cells.

synergistically inhibit the proliferation of human lung cancer A549 cells.[41] The team loaded the water-soluble DOX and water-insoluble PTX into L-HMSNs similarly to how we loaded hydrophilic 5-FU into HMSNs and wrapped hydrophobic PTX in the lipid membrane. However, they did not include any stimulus-responsive materials in the lipid membrane of L-HMSNs, nor did they further modify the hollow mesoporous silica nanospheres. Similarly, other previously reported mesoporous silica nanoparticles (MSN)-based composite carriers have not included stimulus-responsive materials or modifications.[38,40] By contrast, our HMSNs were modified with FA and the polymer p(NIPAAm-*co*-MAA), which endowed HMSNs with

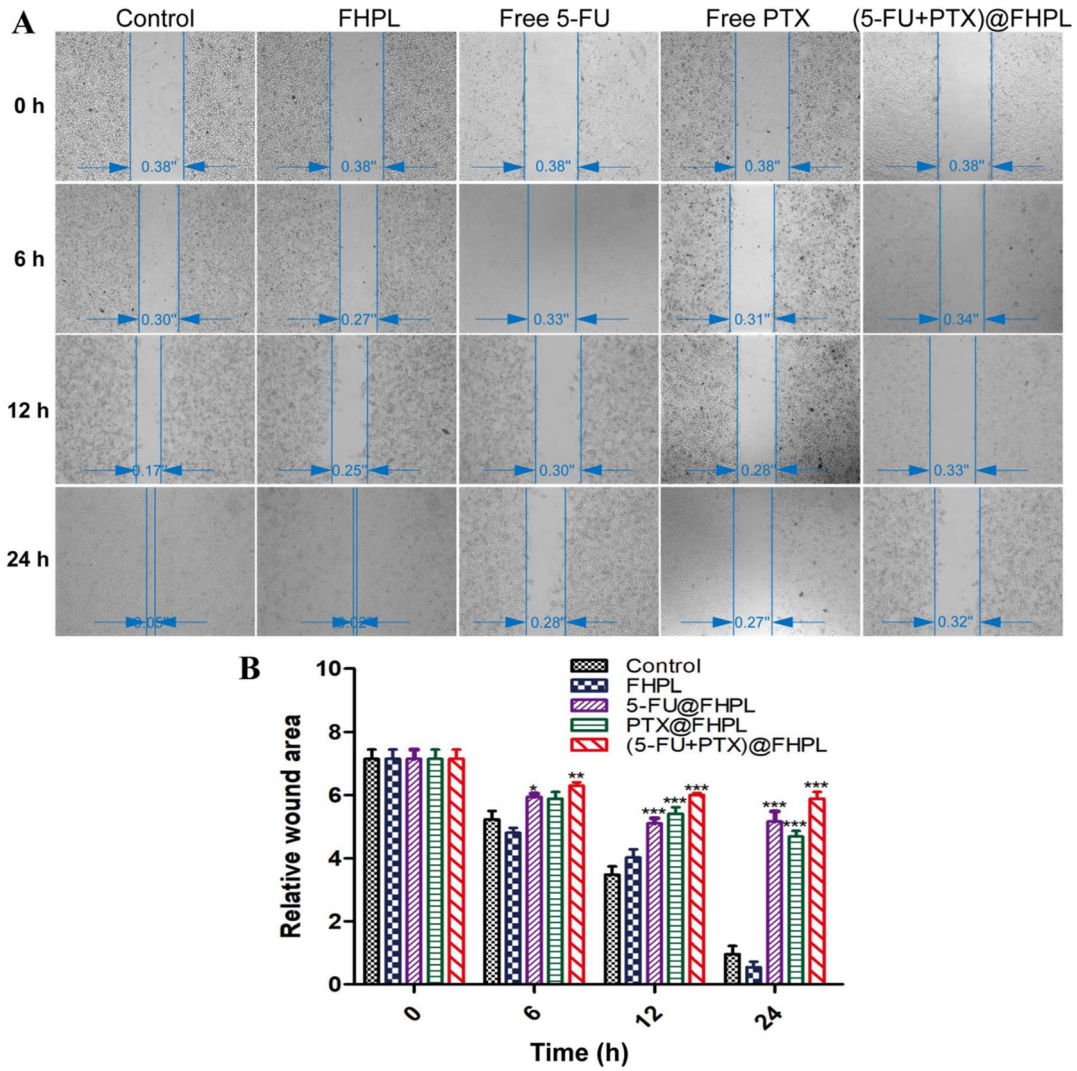

Fig. 12 (A) Wound healing micrographs (magnification, 10×) and (B) relative wound areas after treatment with various formulations for different periods. *$P < 0.05$, **$P < 0.01$, ***$P < 0.001$ *vs.* control (two-way analysis of variance). Data are shown as mean ± SD ($n = 3$). 5-FU, 5-fluorouracil; PTX, paclitaxel.

tumor cell selectivity and tumor microenvironment responsiveness. Another group has developed a light/redox dual-stimuli responsive MSN to target HepG2 cells, but these particles were loaded with single drug, DOX, so it is unclear whether this platform can support combination therapy.[42]

Cancer cell membrane-coated MSNs loaded with superparamagnetic ferroferric oxide and PTX have been reported that can target MDA-MB-231 cells, but the PTX inside the MSNs was released within 1 h, which cannot provide sustained drug release.[43] In contrast, our *in vitro* studies showed that the release of PTX from (5-FU+PTX)@FHPL reached ~50% within 6 h at 41 °C and pH 5.0, while only 40% release of 5-FU was achieved within 12 h under the same conditions. Our drug release properties are consistent with the fact that in combination chemotherapy, PTX is administered before long-term administration of 5-FU.[3,4,6,8] In addition, less than 20% of 5-FU and PTX were released from our (5-FU+PTX)@FHPL at 37 °C and pH 6.8, in contrast to the release of 80% of DOX and 100% of PTX within 12 h from L-HMSNs under the same conditions.[41] These results confirm that drug release from (5-FU+PTX)@FHPL is pH- and temperature-responsive.

Our study provides new insights into the application of 5-FU and PTX in the synergistic treatment of cancer and the development of new anti-tumor treatments. In future studies, we will evaluate the targeting ability, tumor inhibitory effect and biocompatibility of the nanoparticles *in vivo*, as well as explore their potential application to the delivery of other active substances and the treatment of other tumors.

Conclusions

HMSNs modified with FA and a pH- and temperature-responsive polymer were co-loaded with 5-FU and PTX and encapsulated into lipid membranes for synergistic breast cancer treatment. The synthesized nanodelivery system showed good biocompatibility *in vitro*, released both drugs in

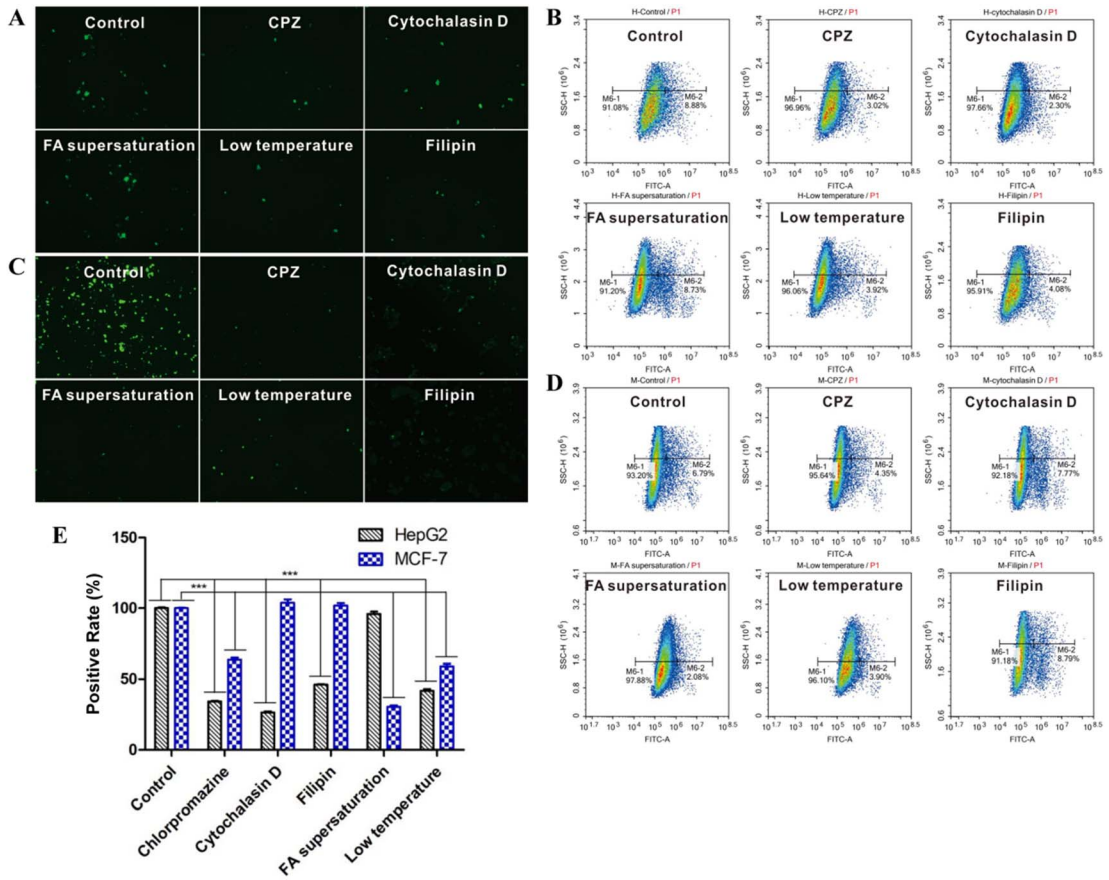

Fig. 13 (A–D) Uptake of FITC@FHPL nanoparticles by (A and B) HepG2 and (C and D) MCF-7 cells after various treatments, as determined by (A and C) fluorescence microscopy and (B and D) flow cytometry. (E) Semi-quantitative analysis of flow cytometry results. ***$P < 0.001$ *vs.* control (two-way analysis of variance). Data are shown as mean ± SD ($n = 3$). CPZ, chlorpromazine; FITC, fluorescein isothiocyanate.

a sustained manner, selectively targeted tumor cells over-expressing α-folate receptors, and improved the effect of free drugs on cell cycle arrest and cell migration, while reducing the necessary dosage and side effects. We expect that this nano-delivery system will provide a new thinking for the development of new strategies for the synergistic treatment of tumors.

Conflicts of interest

There are no conflicts to declare.

Acknowledgements

This work was supported by Sichuan Provincial Medical Research Project (S20059), Sichuan Provincial Administration of Traditional Chinese Medicine Project (2021MS200), the Key Fund Project of Sichuan Provincial Department of Education (No. 17ZA0110) and the Chengdu Medical College Fund Project.

References

1 H. Sung, J. Ferlay, R. L. Siegel, M. Laversanne, I. Soerjomataram, A. Jemal, *et al.*, Global cancer statistics 2020: GLOBOCAN estimates of incidence and mortality worldwide for 36 cancers in 185 countries, *Ca-Cancer J. Clin.*, 2021, **71**(3), 209–249.

2 E. Y. Ko and A. Moon, Natural Products for Chemoprevention of Breast Cancer, *J. Cancer Prev.*, 2015, **20**(4), 223–231.

3 T. Kin, M. Fujihara, Y. Yoshimura, Y. Kajiwara, M. Ito, S. Ohtani, *et al.*, Nanoparticle albumin-bound paclitaxel followed by 5-fluorouracil, epirubicin and cyclophosphamide in neoadjuvant chemotherapy for resectable breast cancer: Phase II trial, *Breast J.*, 2017, **321**, S79–S80.

4 M. Shizuku, M. Shibata, Y. Shimizu, D. Takeuchi and Y. Mizuno, Clinical outcomes of neoadjuvant chemotherapy for patients with breast cancer: Tri-weekly nanoparticle albumin-bound paclitaxel followed by 5-fluorouracil, epirubicin, and cyclophosphamide: a retrospective observational study, *Nagoya J. Med. Sci.*, 2020, **82**(3), 457–467.

5 N. Sathyamoorthy, P. Chintamaneni, S. D. Vankayalu and D. D. Magharla, Biodegradable Polymeric Carrier for Antineoplastic Drugs. Characterization and Sequence Based Cytotoxicity, *Lat. Am. J. Pharm.*, 2017, **36**(7), 1473–1482.

6 Y. Lan, R. Wu, X. Huang, X. Wang, D. Zhong, C. Huang, *et al.*, Paclitaxel, oxaliplatin, 5-fluorouracil and leucovorin combination chemotherapy in patients with recurrent or metastatic gastric cancer, *Tumori J.*, 2018, **104**(1), 22–29.

7 J. Kato, A. Nagahara, K. Iijima, T. Kodani, Y. Higashihara, M. Yoshimura, *et al.*, Phase I study of Paclitaxel, Cisplatin and 5-fluorouracil combination chemotherapy for unresectable/recurrent gastric cancer, *Adv. Med. Sci.*, 2010, **55**(2), 137–142.

8 W. Que, Y. Huang, X. Lin, Y. Lan, X. Gao, X. Wang, *et al.*, Paclitaxel, 5-fluorouracil, and leucovorin combination chemotherapy as first-line treatment in patients with advanced gastric cancer, *Anticancer Drugs*, 2019, **30**(3), 302–307.

9 S. Chatterjee and T. Ooya, Hydrophobic Nature of Methacrylate-POSS in Combination with 2-(Methacryloyloxy)ethyl Phosphorylcholine for Enhanced Solubility and Controlled Release of Paclitaxel, *Langmuir*, 2019, **35**(5), 1404–1412.

10 L. Wang, H. Chen, F. Wang and X. Zhang, The development of peptide-drug conjugates (PDCs) strategies for paclitaxel, *Expert Opin. Drug Delivery*, 2022, 1–15.

11 E. Pretel, J. L. Arias, L. Cabeza, C. Melguizo, J. Prados, M. Mallandrich, *et al.*, Development of biomedical 5-fluorouracil nanoplatforms for colon cancer chemotherapy: Influence of process and formulation parameters, *Int. J. Pharm.*, 2017, **530**(1–2), 155–164.

12 F. Rehan, N. Ahemad, R. A. Islam, M. Gupta, S. H. Gan and E. H. Chowdhury, Optimization and Formulation of Nanostructured and Self-Assembled Caseinate Micelles for Enhanced Cytotoxic Effects of Paclitaxel on Breast Cancer Cells, *Pharmaceutics*, 2020, **12**(10), 984.

13 K. Karthikeyan, C. M. Babu, S. Shaji, A. M. Ashok and C. S. Madhu, Case report on 5-fluorouracil induced cerebrovascular accident, *J. Oncol. Pharm. Pract.*, 2021, **27**(4), 1016–1019.

14 Y. Lin and C. L. Haynes, Impacts of Mesoporous Silica Nanoparticle Size, Pore Ordering, and Pore Integrity on Hemolytic Activity, *J. Am. Chem. Soc.*, 2010, **132**(13), 4834–4842.

15 N. Jatupaiboon, Y. Wang, H. Wu, X. Song, Y. Song, J. Zhang, *et al.*, A facile microemulsion template route for producing hollow silica nanospheres as imaging agents and drug nanocarriers, *J. Mater. Chem. B*, 2015, **3**(16), 3130–3133.

16 W. Feng, L. Chen, X. Zhou, Z. Yin, W. Nie, K. Qiu, *et al.*, A drug delivery system based on novel hollow mesoporous silica nanospheres, *J. Controlled Release*, 2015, **213**, E108–E109.

17 Y. Zhang, Z. Huang, S. Zhang, J. Zhao, Z. Wang, Y. Liu, *et al.*, In vitro cellular uptake of evodiamine and rutaecarpine using a microemulsion, *Int. J. Nanomed.*, 2012, **7**, 2465–2472.

18 G. Zhao and B. L. Rodriguez, Molecular targeting of liposomal nanoparticles to tumor microenvironment, *Int. J. Nanomed.*, 2013, **8**, 61–71.

19 X. Yue and Z. Dai, Recent advances in liposomal nanohybrid cerasomes as promising drug nanocarriers, *Adv. Colloid Interface Sci.*, 2014, **207**(SI), 32–42.

20 Y. J. Kim, J. K. Choi, D. Lee, K. Baek, S. H. Oh and I. S. Lee, Solid-State Conversion Chemistry of Multicomponent Nanocrystals Cast in a Hollow Silica Nanosphere: Morphology-Controlled Syntheses of Hybrid Nanocrystals, *ACS Nano*, 2015, **9**(11), 10719–10728.

21 J. P. Marshalek, P. S. Sheeran, P. Ingram, P. A. Dayton, R. S. Witte and T. O. Matsunaga, Intracellular delivery and ultrasonic activation of folate receptor-targeted phase-change contrast agents in breast cancer cells in vitro, *J. Controlled Release*, 2016, **243**, 69–77.

22 H. Fasehee, R. Dinarvand, A. Ghavamzadeh, M. Esfandyari-Manesh, H. Moradian, S. Faghihi, *et al.*, Delivery of disulfiram into breast cancer cells using folate-receptor-targeted PLGA-PEG nanoparticles: *in vitro* and *in vivo* investigations, *J. Nanobiotechnol.*, 2016, 14.

23 H. H. Dong, S. B. Cheol and C. H. Suk, Doxorubicin-encapsulated thermosensitive liposomes modified with poly(N-isopropylacrylamide-*co*-acrylamide): drug release behavior and stability in the presence of serum, *Eur. J. Pharm. Biopharm.*, 2006, **62**(1), 110.

24 A. Garcia-Penas, Y. Wang, A. Munoz-Bonilla, M. Fernandez-Garcia and F. J. Stadler, Lower Critical Solution Temperature Sensitivity to Structural Changes in Poly(N-Isopropyl Acrylamide) Homopolymers, *J. Polym. Sci., Polym. Phys.*, 2019, **57**(20), 1386–1393.

25 Y. Gao, J. Yang, Y. Ding and X. Ye, Effect of Urea on Phase Transition of Poly(N-isopropylacrylamide) Investigated by Differential Scanning Calorimetry, *J. Phys. Chem. B*, 2014, **118**(31), 9460–9466.

26 T. Chou, Drug Combination Studies and Their Synergy Quantification Using the Chou-Talalay Method, *Cancer Res.*, 2010, **70**(2), 440–446.

27 V. Banerjee, N. Sharda, J. Huse, D. Singh, D. Sokolov, S. J. Czinn, *et al.*, Synergistic potential of dual andrographolide and melatonin targeting of metastatic colon cancer cells: Using the Chou-Talalay combination index method, *Eur. J. Pharmacol.*, 2021, 897.

28 A. K. A. Wiggins, S. Kharotia, J. K. Mason and L. U. Thompson, alpha-Linolenic Acid Reduces Growth of Both Triple Negative and Luminal Breast Cancer Cells in High and Low Estrogen Environments, *Nutr. Cancer*, 2015, **67**(6), 1001–1009.

29 S. Lyu, H. Liu, X. Liu, S. Liu, Y. Wang, Q. Yu, *et al.*, Interrelation of androgen receptor and miR-30a and miR-30a function in ER-, PR-, AR(+) MDA-MB-453 breast cancer cells, *Oncol. Lett.*, 2017, **14**(4), 4930–4936.

30 L. Chun-Chi, Y. Park Ann and G. Jun-Lin, *In vitro* scratch assay: a convenient and inexpensive method for analysis of cell migration in vitro, *Nat. Protoc.*, 2007, **2**(2), 329–333.

31 Z. Jing, H. Xu, X. Chen, Q. Zhong, J. Huang, Y. Zhang, *et al.*, The Proton-Sensing G-Protein Coupled Receptor GPR4 Promotes Angiogenesis in Head and Neck Cancer, *PLoS One*, 2016, **11**(4), e0152789.

32 X. Cheng, J. Gao, J. Li, G. Cheng, M. Zou and H. Piao, *In Vitro-In Vivo* Correlation for Solid Dispersion of a Poorly Water-Soluble Drug Efonidipine Hydrochloride, *AAPS PharmSciTech*, 2020, **21**(5), 160.

33 A. Jain and S. K. Jain, In vitro release kinetics model fitting of liposomes: An insight, *Chem. Phys. Lipids*, 2016, **201**, 28–40.
34 S. Dubey, D. Gusain and Y. C. Sharma, Kinetic and isotherm parameter determination for the removal of chromium from aqueous solutions by nanoalumina, a nanoadsorbent, *J. Mol. Liq.*, 2016, **219**, 1–8.
35 K. Yadav, D. Yadav and A. K. Srivastava, Evaluation of hydrophilic, hydrophobic and waxy matrix excipients for sustained release tablets of Venlafaxine hydrochloride, *Drug Dev. Ind. Pharm.*, 2013, **39**(8), 1197–1206.
36 M. K. Gupta, D. Prakash and B. Mishra, Biodegradable microparticulate drug delivery system of diltiazem HCl, *Braz. J. Pharm. Sci.*, 2012, **48**(4), 699–709.
37 H. Geng, W. Chen, Z. P. Xu, G. Qian, J. An and H. Zhang, Shape-Controlled Hollow Mesoporous Silica Nanoparticles with Multifunctional Capping for *In Vitro* Cancer Treatment, *Chem.–Eur. J.*, 2017, **23**(45), 10878–10885.
38 Y. Feng, N. Li, H. Yin, T. Chen, Q. Yang and M. Wu, Thermo- and pH-responsive, Lipid-coated, Mesoporous Silica Nanoparticle-based Dual Drug Delivery System To Improve the Antitumor Effect of Hydrophobic Drugs, *Mol. Pharmaceutics*, 2019, **16**(1), 422–436.
39 S. Guo, Y. Wang, L. Miao, Z. Xu, C. M. Lin, Y. Zhang, *et al.*, Lipid-Coated Cisplatin Nanoparticles Induce Neighboring Effect and Exhibit Enhanced Anticancer Efficacy, *ACS Nano*, 2013, **7**(11), 9896–9904.
40 H. Meng, M. Wang, H. Liu, X. Liu, A. Situ, B. Wu, *et al.*, Use of a Lipid-Coated Mesoporous Silica Nanoparticle Platform for Synergistic Gemcitabine and Paclitaxel Delivery to Human Pancreatic Cancer in Mice, *ACS Nano*, 2015, **9**(4), 3540–3557.
41 Y. Qiu, C. Wu, J. Jiang, Y. Hao, Y. Zhao, J. Xu, *et al.*, Lipid-coated hollow mesoporous silica nanospheres for co-delivery of doxorubicin and paclitaxel: Preparation, sustained release, cellular uptake and pharmacokinetics, *Mater. Sci. Eng., C*, 2017, **71**, 835–843.
42 Y. Wu, Z. Xu, W. Sun, Y. Yang, H. Jin, L. Qiu, *et al.*, Co-responsive smart cyclodextrin-gated mesoporous silica nanoparticles with ligand-receptor engagement for anti-cancer treatment, *Mater. Sci. Eng., C*, 2019, 103.
43 D. Cai, L. Liu, C. Han, X. Ma, J. Qian, J. Zhou, *et al.*, Cancer cell membrane-coated mesoporous silica loaded with superparamagnetic ferroferric oxide and Paclitaxel for the combination of Chemo/Magnetocaloric therapy on MDA-MB-231 cells, *Sci. Rep.*, 2019, **9**, 14475.